ENHANCED RETINAL IMAGE REGISTRATION ACCURACY USING EXPECTATION MAXIMISATION AND VARIABLE BIN-SIZED MUTUAL INFORMATION

Parminder Singh Reel[†]   *Laurence S. Dooley*[†]   *K.C.P Wong*[†]   *Anko Börner*[⋆]

[†]Department of Computing and Communications, The Open University, Milton Keynes, United Kingdom
[⋆]Optical Sensor Systems, German Aerospace Center (DLR), Berlin, Germany
Email: [†]{*parminder.reel, laurence.dooley, k.c.p.wong*}*@open.ac.uk*, [⋆]*anko.boerner@dlr.de*

ABSTRACT

While *retinal images* (RI) assist in the diagnosis of various eye conditions and diseases such as glaucoma and diabetic retinopathy, their innate features including low contrast homogeneous and non-uniformly illuminated regions, present a particular challenge for *retinal image registration* (RIR). Recently, the hybrid similarity measure, *Expectation Maximization for Principal Component Analysis with Mutual Information* (EMPCA-MI) has been proposed for RIR. This paper investigates incorporating various fixed and adaptive bin size selection strategies to estimate the probability distribution in the *mutual information* (MI) stage of EMPCA-MI, and analyses their corresponding effect upon RIR performance. Experimental results using a clinical mono-modal RI dataset confirms that adaptive bin size selection consistently provides both lower RIR errors and superior robustness compared to the empirically determined fixed bin sizes.

Index Terms— Image registration, ophthalmological image processing, principal component analysis, mutual information, expectation-maximization algorithms.

1. INTRODUCTION

Image registration is an integral process in many computer vision and image processing applications [1], [2], with the registration of medical images assisting in disease diagnosis and treatment planning [3] for various regions in human anatomy including the brain and retina. *Retinal image registration* (RIR) spatially aligns the vessel structures of the retina in order to assist in ophthalmology, particularly in tracking the advancement of diagnosed eye conditions and diseases such as myopia, glaucoma and diabetic retinopathy [4]. RIR is especially challenging because *retinal images* (RI) generally have non-uniform intensity distributions allied with the presence of large homogeneous non-vascular regions. RI quality can also be compromised by the presence of different pathologies like haemorrhages and retinal scars caused by laser treatment [5].

Many existing feature-based RIR techniques are not sufficiently robust due to their dependency on the quality of RI segmentation and the extracted features. Similarly, intensity-based methods including *mutual information* (MI) [6] which use only individual and joint probabilities of pixels, exhibit degraded RIR performance because of the aforementioned RI attributes [7]. It has been reported [6] that a more accurate MI value can be achieved during registration by selecting the most appropriate bin size for probability estimation. From a RI perspective, the latent mage quality means that determining the best bin size for MI computation can play a vital role in the overall RIR performance, though any improvement may be limited since MI does not include spatial information. Existing hybrid-based techniques which do integrate spatial information along with MI have not employed bin size selection for RIR. Given the challenging features, bin size selection in calculating MI in hybrid-based techniques affords a fertile opportunity to investigate its impact on RIR accuracy.

This paper analyses the effect of introducing either a fixed or adaptive bin size selection strategy into the hybrid-based similarity measure *Expectation Maximization for Principal Component Analysis with Mutual Information* (EMPCA-MI) [8] algorithm. EMPCA-MI incorporates RI spatial information together with a fixed 256 bins probability distribution for MI, to achieve effective RIR with low computational overheads. Numerical and qualitative results for different fixed and adaptive bin size selections for EMPCA-MI using a clinical dataset of 44 mono-modal RI pairs containing different pathologies, corroborates that improved RIR accuracy and robustness is achieved, with adaptive bin selection approaches consistently providing lower registration errors. The remainder of the paper is organised as follows: Section 2 presents a review of existing RIR techniques, while Section 3 initially reviews the EMPCA-MI-based RIR framework before describing various fixed and adaptive bin size selection techniques for MI computation and their integration into EMPCA-MI. Section 4 outlines the experimental set-up and analyses the corresponding RIR performance, with some concluding comments being given in Section 5.

2. PREVIOUS WORK

RIR is broadly classified into *feature*, *intensity* and *hybrid* based techniques [7]. While feature-based approaches primarily use optical disk [9], fovea [10] and vascular structural details [11], [12] from the RI, intensity-based techniques focus on pixel intensity information using similarity measures such as cross correlation, phase correlation or MI [6], [13]. MI establishes a statistical relationship between the intensity values of the RI and while it is popular in the medical image registration domain, it is not very effective for RIR because of the aforementioned RI characteristics
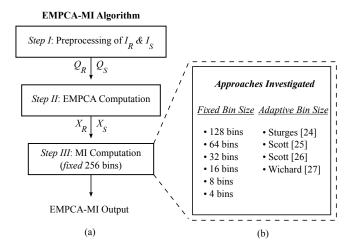
Fig. 1. (a) EMPCA-MI Algorithm [8] (b) various different bin size selection techniques investigated in *Step III*.

[14]. The inherently large homogeneous regions in RI mean that choosing a high number of bins for probability distribution estimation can produce many empty bins and an inaccurate MI value, thus selecting the most appropriate bin size for MI computation has a significant impact on overall RIR performance [15], with normally fewer bins being either empirically [16–18] or statistically [19] used.

Empirically testing fixed bin sizes in the range from 256 to 4 bins, in a binary-reducing (2^{-N}) in the MI computation for RIR, has been proposed in [16–18] and [20]. In contrast, the statistics literature addresses optimal bin size selection for probability distribution estimation [21, 22] which has been successfully employed for MI in both RIR [19] and remote sensing registration applications [23]. Sturges [24] defined the bin size by assuming data was normally distributed so it could be represented as a binomial distribution, while Scott [25] based bin selection upon the standard deviation of the data. While both rules assume normal distributed data, [26] extended the fundamental theory to consider skewed data by incorporating a *skewness* factor. Another extension proposed by Wichard [27], included a *kurtosis* measure to calculate the optimal number of bins for accurate probability distribution. While incorporating both skewness and kurtosis into the bin size selection rules [26, 27] provides greater robustness for RI data, which otherwise does not represent the RI characteristics, it also has computational implications for RIR.

Legg [15] concluded that despite using statistical bin size selection methods, MI does not always provide a reliable RIR similarity measure because it lacks spatial information, which has been included in hybrid methods like *regional* MI [28]. EMPCA-MI [8] is hybrid-based similarity measure which has recently been shown to exhibit superior RIR robustness in the presence of non-uniform intensity and noise, outperforming other feature, intensity and hybrid-based techniques [8], [29–32] by effectively combining spatial information with MI in a fixed 256 bin arrangement. The challenging characteristics of RI provided the motivation to seek to develop a formal mechanism for the best bin size selection [16–19] for the MI computation block of EMPCA-MI and to analyse its corresponding RIR performance.

3. EMPCA-MI FOR RIR USING FIXED AND ADAPTIVE BIN SIZE SELECTION

3.1. EMPCA-MI based RIR Framework

RIR involves the geometric transformation of a source RI (I_S) to attain the best physical alignment with a reference target image (I_R). An optimization method is applied to maximize some predefined similarity measure with known transformations between the I_R and I_S dataset.

EMPCA-MI is a new similarity measure for RIR, which efficiently incorporates spatial information together with MI without incurring high computational overheads [8]. Fig. 1(a) displays the three constituent EMPCA-MI processing blocks, which are respectively; input data rearrangement, EMPCA and MI calculation. Both I_R and I_S are pre-processed (*Step I*) as Q_R and Q_S using a neighbourhood radius r, so the spatial and intensity information is preserved [8]. The first P principal components X_R and X_S of the respective I_R and I_S images are then iteratively computed from Q_R and Q_S using EMPCA in *Step II*, instead of solving the whole covariance matrix. Finally the MI [6] is calculated using 256 bins between X_R and X_S in *Step III*, with a higher MI value meaning the images are better aligned. In [8], $r=1$ is chosen because of the intrinsically large homogeneous regions in RI and only the first principal component is considered, i.e., $P=1$ since this is the direction of highest variance and represents the most dominant feature in any RI region. Mathematically, EMPCA-MI can be formally expressed as:

$$EMPCA - MI(I_R, I_S) = \sum_{X_R, X_S} p(X_R, X_S) \log \frac{p(X_R, X_S)}{p(X_R), p(X_S)} \quad (1)$$

where $p(X_R)$ and $p(X_S)$ are the individual probabilities of X_R and X_S respectively, while $p(X_R, X_S)$ is their joint probability.

3.2. Bin Size Selection for MI Computation

In *Step III* of the EMPCA-MI algorithm, MI is calculated between the principal components X_R and X_S to determine the final EMPCA-MI value using a fixed bin size of 256 bins. This subsection examines different fixed and adaptive bin size selection approaches which can be incorporated for individual and joint probability estimation (See (1)) for more accurate MI computation between X_R and X_S as shown in *Step III*. These are summarised in Fig. 1(b).

The first set of approaches investigated consisted of empirically decreasing the fixed bin sizes from 256 in the original EMPCA-MI [8] algorithm to 128, 64, 32, 16, 8 and 4 bins [16–18] respectively and analysing the corresponding impact on RIR performance. Intuitively, reducing the bin number improves the probability distribution estimation since X_R and X_S data are now distributed across fewer numbers of sparse bins. Conversely, radically reducing the number of bins leads to a loss of the unique features of X_R and X_S. Computation overheads for all the fixed bin size approaches are minimal since bin size is predefined and not iteratively computed, though more bins require more computation time for calculating the individual and joint probability in (1).

The next bin size selection category [24–27] investigated were statistically-based and adaptive in nature, i.e. they are dependent

on the statistical characteristics of X_R and X_S. Both [24] and [25] assume X_R and X_S to be normally distributed, while [26] and [27] include the higher-order moments (skewness and kurtosis) so both X_R and X_S can be more accurately modelled and their flat or peak distribution nature better represented in the bin size selection strategy. Inclusion of higher-order moments impacts on the computational times for [26] and [27], while it is marginally lower for [24] and [25].

Overall, adaptive bin size selection approaches incur higher computational costs because of their iterative nature, with the bin size being computed every RIR iteration.These various MI computation approaches for EMPCA-MI provide a mechanism for determining the best number of bins for accurate MI calculation. In comparison to the fixed 256 bins EMPCA-MI algorithm, they introduce a new degree-of-freedom based on the RI statistical characteristics. A fixed bin approach (along with the original 256 bins based EMPCA-MI [8]) and four adaptive selection methods [24–27] have been incorporated into the MI computation (*Step III*) of EMPCA-MI (see Figs 1(a) and (b)), and a comparative analysis undertaken to evaluate their impact on the overall RIR performance, as will be evidenced in the next section.

4. EXPERIMENTAL EVALUATION

4.1. Experimental Setup and Clinical Dataset

To analyse different bin size selections in the MI computation block of the EMPCA-MI framework in Fig. 1(b), a mono-modal clinical dataset comprising 44 RI pairs of colour fundus images were used [33]. Each colour fundus image had a spatial resolution of *3504 × 2336* pixels, a *60°* field of view and were acquired by a Canon CF-60UV with digital camera Canon EOS 20D. Each RI image contained non-uniform illumination, low contrast and different pathologies including haemorrhages, retinal scars and clumping of the dark pigment which all accentuated the RIR challenge. While these varying RI characteristics mean this dataset is very challenging, it also affords the opportunity to investigate the impact bin size selection upon the robustness of RIR accuracy. RIR was undertaken upon only the green channel, since this has the highest contrast compared with the red and blue channels, which are often saturated and contain acquisition noise [7].

RI acquisition inherently leads to distortion between I_S and I_R, which can be modelled as a *similarity transformation*, which is a special form of the global affine transform [34]. This represents the RI distortion as either eye or camera (t_x, t_y for x and y translation and rotational θ) motion, with the magnification changes resulting from either using different equipment or the motion in the direction of the optical axis, being modelled as a uniform scaling S [5] in combination with bi-cubic interpolation [34]. Since reference images were not available for this RI dataset, to establish the requisite ground truth, all RI were misregistered by (*100, 100, 45°, 0.8*) represented by (t_x, t_y, θ, S) to simulate a particularly challenging registration scenario, with the original images being then considered as the sensed RI. To automatically determine the RIR parameters, Powells multidimensional direction set method was applied along with Brent optimization [35] for line minimization, because it provided a local search which is accurate, fast and

Bin Sizes	Mean Errors				RE	ART
	Δt_x	Δt_y	$\Delta\theta$	ΔS	(pixels)	(secs)
Fixed						
256 *bins* [8]	-4.0	8.0	2.8	0.08	106.35	1.32
128 *bins*	6.0	4.5	2.6	0.12	96.25	1.24
64 *bins*	5.5	-9.5	1.9	0.06	70.15	1.18
32 *bins*	5.0	-8.5	1.4	0.03	51.82	1.10
16 *bins*	5.0	7.0	-1.5	0.04	55.97	0.91
8 *bins*	-3.0	6.0	1.2	0.08	65.10	0.89
4 *bins*	8.0	7.0	2.1	0.03	77.35	0.86
Adaptive						
Sturges [24]	5.0	-8.0	-1.8	0.04	51.77	1.28
Scott [25]	7.0	6.0	-1.3	0.05	48.60	1.36
Scott [26]	2.0	4.0	1.2	0.03	39.20	3.14
Wichard [27]	9.0	-3.0	-0.9	0.02	38.65	3.98

Table 1. *RE* and average runtimes (ART) for EMPCA-MI based RIR for different fixed and adaptive bin size selections. Δt_x, Δt_y, $\Delta\theta$, ΔS are the similarity transformation errors.

especially suited to RIR [2]. The respective tolerance thresholds for the Powell and Brent criteria were 10^{-5} and 10^{-3} [2], with the maximum number of iterations being 200.

To quantify the results, the *registration errors* (RE) were computed as the mean distance error (measured in pixels) between the four corner points of the reference and sensed images [19], [23]. In addition, the EMPCA-MI *average run time* (ART) was calculated for every RIR iteration for both the various fixed and adaptive bin size approaches. the iterations of the RIR process in case of all fixed and adaptive approaches. All experiments were performed upon an Ubuntu 10.04 (*lucid*) with 2.93 GHz Intel Core and 3GB RAM, and the assorted algorithms implemented in MATLAB.

4.2. Results Discussion

Table 1 summarizes the *RE* and *ART* results for EMPCA-MI based RIR, when integrated with different *fixed* and *adaptive* bin size selection strategies. It is evident from Table 1 that in terms of RIR accuracy, the Wichard adaptive approach [27] has the lowest *RE* of 33.65 pixels since it iteratively computes the best bin size based upon the characteristics of X_R and X_S for each RI pair. In terms of the empirical fixed bin size approaches, 32 bins performed best with a *RE* of 51.82 pixels.

A detailed *RE* boxplot covering the results for different fixed and adaptive techniques is displayed in Fig 2. This consists of a bounding box defining the interquartile range with a bar across representing the median and whiskers defining the *RE* range. The boxplot interestingly reveals a trend as it is clear the *RE* decreases as the fixed bin size is reduced from the standard 256 bins of the original EMPCA-MI [8] to 32, before it then starts increasing again when the bin number is further reduced. The reason for this is that when large numbers of bins are used in the MI computation in *Step III*, there is a tendency to have more sparsely-populated bins within the joint histogram which leads to poorly estimated entropy. Conversely, for smaller bin sizes (16, 8 and 4), unique features will
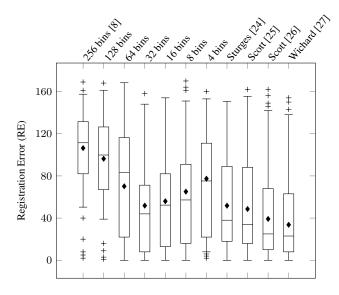
Fig. 2. RE Boxplot for EMPCA-MI based RIR. *Mean* and *outliers* are denoted by the *diamond* and *cross* shapes respectively.

tend to become assigned to the same bin, leading to a corresponding degradation in RIR performance. So for this clinical RI dataset, 32 bins is the best size within the fixed bin approaches. This may vary for different RI datasets depending upon the precise characteristics of the RI dataset, which highlights one of the limitations of adopting a fixed bin size approach.

For adaptive bin size selection, the results show that Wichard's method [27] achieved the lowest *RE* followed by Scott's adaptive strategy [26]. These techniques include higher-order moments of kurtosis and skewness of the data distribution which assists to better model the RI characteristics. In contrast, the performance of both [24] and [25] is much lower which is due to the fact that their underlying assumption is that the RI data is normally distributed which leads to inaccurate MI computation and higher *RE*.

In terms of computational overheads, it is evident from Table 1 that the *ART* decreases for smaller fixed bin sizes i.e., 1.32*sec* to 0.86*sec* for 256 to 4 bins respectively, due to the lower individual and joint probability computational times incurred for smaller bins. Similarly, higher *ART* of 3.98*sec* and 3.14*sec* are respectively observed for the two adaptive approaches of [27] and [26] since they required the calculation of higher-order moments in their bin size selections for determining the respective individual and joint probabilities in (1).

Fig. 3 shows zoomed in examples of the qualitative RIR results for challenging RI pair #12, using the checkerboard overlaying method [2], with I_R and I_S in light and dark respectively. This RI pair is especially challenging as it includes assorted laser treatment scars along with low contrast and large homogeneous regions. The superior continuity of the vessel structures is evident in the best adaptive approach [27] and fixed 32 bins and validates their effective qualitative RIR performance in contrast to employing either 256 [8] or 4 bins in EMPCA-MI.
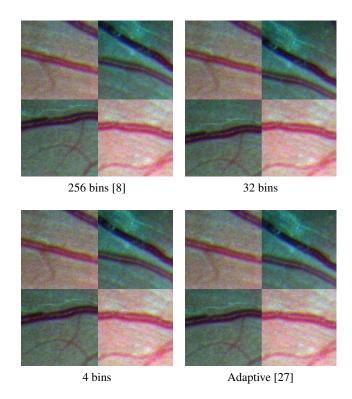

256 bins [8] 32 bins

4 bins Adaptive [27]

Fig. 3. Checkerboard overlay [2] illustration of RI pair #12 for various bin size selections.

5. CONCLUSION

This paper has analysed different fixed and adaptive bin size selection strategies within the *Expectation Maximization for Principal Component Analysis with Mutual Information* (EMPCA-MI) similarity measure, for *retinal image registration* (RIR). RIR is especially challenging because of inherent image characteristics of low contrast, non-uniform illumination and large homogeneous regions. Quantitative and qualitative RIR results for a monomodal clinical retinal image dataset confirm that by adopting adaptive bin size selection to computing the MI value in EMPCA-MI consistently outperformed fixed bin size strategies in terms of the registration accuracy and robustness.

6. REFERENCES

[1] J. B. A. Maintz and M. A. Viergever, "A survey of medical image registration," *Medical Image Analysis*, vol. 2, no. 1, pp. 1–36, Mar. 1998.

[2] B. Zitová and J. Flusser, "Image registration methods: a survey," *Image Vision Comput.*, vol. 21, no. 11, pp. 977–1000, Oct. 2003.

[3] D. L. G. Hill, P. G. Batchelor, M. Holden, and D. J. Hawkes, "Medical image registration," *Phys. Med. Biol.*, vol. 46, no. 3, pp. R1–R45, Mar. 2001.

[4] C. Sanchez-Galeana, C. Bowd, E. Z. Blumenthal, P. A. Gokhale, L. M. Zangwill, and R. N. Weinreb, "Using optical

imaging summary data to detect glaucoma," *Ophthalmology*, vol. 108, no. 10, pp. 1812–1818, Oct. 2001.

[5] P. J. Saine and M. E. Tyler, *Ophthalmic photography : retinal photography, angiography, and electronic imaging*, Butterworth-Heinemann, Boston, 2002.

[6] F. Maes, A. Collignon, D. Vandermeulen, G. Marchal, and P. Suetens, "Multimodality image registration by maximization of mutual information," *IEEE Trans. Med. Imag.*, vol. 16, no. 2, pp. 187–198, Apr. 1997.

[7] F. Laliberte, L. Gagnon, and Y. Sheng, "Registration and fusion of retinal images-an evaluation study," *IEEE Trans. Med. Imag.*, vol. 22, no. 5, pp. 661 –673, May 2003.

[8] P. S. Reel, L. S. Dooley, K. C. P. Wong, and A. Börner, "Robust retinal image registration using expectation maximisation with mutual information," in *(ICASSP)*, May 2013, pp. 1118–1122.

[9] J. Xu, O. Chutatape, E. Sung, C. Zheng, and P. Chew Tec Kuan, "Optic disk feature extraction via modified deformable model technique for glaucoma analysis," *Pattern Recogn.*, vol. 40, no. 7, pp. 2063–2076, July 2007.

[10] H. Li and O. Chutatape, "Automated feature extraction in color retinal images by a model based approach," *IEEE Trans. Biomed. Eng.*, vol. 51, no. 2, pp. 246 –254, Feb. 2004.

[11] S. Gharabaghi, S. Daneshvar, and M. Sedaaghi, "Retinal image registration using geometrical features," *J. Digit. Imaging*, vol. 26, no. 2, pp. 248–258, 2013.

[12] L. Chen, Y. Xiang, Y. Chen, and X. Zhang, "Retinal image registration using bifurcation structures," in *(ICIP)*, Sept. 2011, pp. 2169 –2172.

[13] M. Skokan, A. Skoupy, and J. Jan, "Registration of multimodal images of retina," in *(EMBS)*, 2002, vol. 2, pp. 1094–1096.

[14] L. Kubecka and J. Jan, "Registration of bimodal retinal images - improving modifications," in *(IEMBS)*, Sept. 2004, vol. 1, pp. 1695 –1698.

[15] P.A. Legg, P.L. Rosin, D. Marshall, and J.E. Morgan, "Improving accuracy and efficiency of mutual information for multi-modal retinal image registration using adaptive probability density estimation," *Comput. Med. Imag. Grap.*, 2013.

[16] N. Ritter, R. Owens, J. Cooper, R.H. Eikelboom, and P.P. van Saarloos, "Registration of stereo and temporal images of the retina," *IEEE Trans. Med. Imag.*, vol. 18, no. 5, pp. 404–418, 1999.

[17] Haewon Nam, Rosemary A. Renaut, Kewei Chen, Hongbin Guo, and Gerald E. Farin, "Improved inter-modality image registration using normalized mutual information with coarse-binned histograms," *Commun. Numer. Meth. En.*, vol. 25, no. 6, pp. 583–595, 2009.

[18] Juan Kang, Chuangbai Xiao, M. Deng, Jing Yu, and Haifeng Liu, "Image registration based on harris corner and mutual information," in *(EMEIT)*, 2011, vol. 7, pp. 3434–3437.

[19] P. A. Legg, P. L. Rosin, D. Marshall, and J. E. Morgan, "Improving accuracy and efficiency of registration by mutual information using sturges' histogram rule," in *(MIUA)*, pp. 26–30. Jan. 2007.

[20] Yang-Ming Zhu and Steven M. Cochoff, "Influence of implementation parameters on registration of mr and spect brain images by maximization of mutual information," *J. Nucl. Med.*, vol. 43, no. 2, pp. 160–166, 2002.

[21] L. Birgé and Y. Rozenholc, "How many bins should be put in a regular histogram," *ESAIM: Probability and Statistics*, vol. 10, pp. 24–45, 10 2006.

[22] P. L. Davies, U. Gather, D. Nordman, and H. Weinert, "Constructing a regular histogram : a comparison of methods," Technical Reports 2007,14, TU Dortmund, 2007.

[23] A. Dame and E. Marchand, "Accurate real-time tracking using mutual information," in *(ISMAR)*, 2010, pp. 47–56.

[24] Herbert A. Sturges, "The choice of a class interval," *J. Am. Stat. Assoc.*, vol. 21, no. 153, pp. 65–66, 1926.

[25] D. W. Scott, "On optimal and data-based histograms," *Biometrika*, vol. 66, no. 3, pp. 605–610, 1979.

[26] D. W. Scott, *Multivariate Density Estimation: Theory, Practice, and Visualization*, John Wiley & Sons, Inc., 1992.

[27] J.D. Wichard, R. Kuhne, and A. ter Laak, "Binding site detection via mutual information," in *(IEEE FUZZ)*, 2008, pp. 1770–1776.

[28] D. B. Russakoff, C. Tomasi, T. Rohlfing, and C. R. Maurer, "Image similarity using mutual information of regions," in *(ECCV)*, vol. 3023, pp. 596–607. Springer, 2004.

[29] P. S. Reel, L. S. Dooley, and K. C. P. Wong, "A new mutual information based similarity measure for medical image registration," in *(IET IPR)*, July 2012, pp. 1 –6.

[30] P. S. Reel, L. S. Dooley, and K. C. P. Wong, "Efficient image registration using fast principal component analysis," in *(ICIP)*, 2012, pp. 1661–1664.

[31] P. S. Reel, L. S. Dooley, K. C. P. Wong, and A. Börner, "Multimodal retinal image registration using fast principal component analysis hybrid-based similarity measure," in *(ICIP)*, 2013, pp. 1428–1432.

[32] P. S. Reel, L. S. Dooley, K. C. P. Wong, and Anko Börner, "Fast EM principal component analysis image registration using neighbourhood pixel connectivity," in *CAIP '13*, vol. 8047, pp. 270–277. Springer, 2013.

[33] R. Kolar and P. Tasevsky, "Registration of 3d retinal optical coherence tomography data and 2d fundus images," in *BIR*, number 6204 in LNCS, pp. 72–82. Springer, Jan. 2010.

[34] L. G. Brown, "A survey of image registration techniques," *ACM Comput. Surv.*, vol. 24, no. 4, pp. 325–376, Dec. 1992.

[35] W. H. Press, S. A. Teukolsky, W. T. Vetterling, and B. P. Flannery, *Numerical Recipes 3rd Edition: The Art of Scientific Computing*, Cambridge University Press, 3 edition, Sept. 2007.